Biomass Conversion

Deutsche Ausgabe: DOI: 10.1002/ange.201604108
Internationale Ausgabe: DOI: 10.1002/anie.201604108

From Biomass-Derived Furans to Aromatics with Ethanol over Zeolite

Ivo F. Teixeira[+], Benedict T. W. Lo[+], Pavlo Kostetskyy, Michail Stamatakis, Lin Ye, Chiu C. Tang, Giannis Mpourmpakis, and Shik Chi Edman Tsang**

Abstract: *We report a novel catalytic conversion of biomass-derived furans and alcohols to aromatics over zeolite catalysts. Aromatics are formed via Diels–Alder cycloaddition with ethylene, which is produced in situ from ethanol dehydration. The use of liquid ethanol instead of gaseous ethylene, as the source of dienophile in this one-pot synthesis, makes the aromatics production much simpler and renewable, circumventing the use of ethylene at high pressure. More importantly, both our experiments and theoretical studies demonstrate that the use of ethanol instead of ethylene, results in significantly higher rates and higher selectivity to aromatics, due to lower activation barriers over the solid acid sites. Synchrotron-diffraction experiments and proton-affinity calculations clearly suggest that a preferred protonation of ethanol over the furan is a key step facilitating the Diels–Alder and dehydration reactions in the acid sites of the zeolite.*

Over the past century our society has become heavily dependent on fossil-fuel sources, such as coal, gas, and oil to produce our daily needed energy and chemicals.[1–3] The carbon dioxide produced by these non-renewable carbon sources has been significantly altering the climate on Earth[2] and our heavy reliance makes them more expensive and less abundant.[1–3] Conversion of lignocellulosic biomass into renewable fuels and chemicals has attracted significant attention as a key technology to enable the replacement of petroleum.[4] Lignocellulosic biomass is the most promising renewable carbon energy source, as it is widely available around the world at a relatively low cost. It is composed of three main fractions: cellulose, hemicellulose, and lignin.[5] Although it is the most abundant plant material resource, its exploitation has been limited by its composite nature and rigid structure.[6] In view of these facts, the conversion of biomass feedstocks into valuable products has been investigated, usually in multistep processes using platform molecules as intermediates.[7] Bio-derived furans, such as furfural (FF), furfuryl alcohol (FA), 2-methylfuran (MF), and 2,5-dimethylfuran (DMF), are important platform molecules that can be produced by hydrolysis and subsequent dehydration of hemicellulose and cellulose from biomass at good yields.[8] It has recently been demonstrated that these platform molecules with a furan ring can be converted into aromatics (particularly *p*-xylene) by a Diels–Alder cycloaddition with an alkene (usually ethylene or propylene), followed by dehydration over a moderately acidic zeolite.[9–12] However, this process is not completely renewable, since the alkene gas added usually comes from fossil sources.[9–11] Another disadvantage of this batch synthesis is the need to apply high ethylene gas pressure from gas store,[9–11] which makes the process more cumbersome and less safe to handle. Herein, we have investigated the catalytic conversion of 2,5-dimethylfuran (DMF) into aromatics by Diels–Alder cycloaddition with ethylene, generated in situ by dehydration of bio-derived ethanol over zeolite. Reactions were carried out in a one-pot synthesis, using liquid ethanol and furan in a batch reactor, without the need for processing high-pressure ethylene. It is generally accepted that ethylene can be produced by the dehydration of ethanol over acid or basic sites of the zeolites.[13] Although slower kinetics would be expected in the conversion of DMF using ethanol instead of ethylene due to the competition for the active sites (e.g. ethanol dehydration also takes place on acid sites). In contrast, we achieve much higher rates and lower activation barriers due to hitherto unreported steps for the coupling of ethanol and furan to form aromatics. The new process using ethanol as a renewable dienophile is demonstrated to be technical and economically more attractive in the conversion of furans into aromatics over zeolites.

First, the reaction conditions for the ethanol/DMF reaction over zeolite were carefully considered as similar to those reported for ethylene/DMF reactions in the literature ensuring no mass transfer limitations, see Supporting Information.[9–11] Figure 1 shows a high conversion of DMF after it is mixed with liquid ethanol at 1:1 mole ratio over all zeolites (ca. 80–95%, see Figure S2). The condensable products include the desirable product, *p*-xylene from the Diels–Alder and dehydration reactions (Scheme 1), alkylated aromatics (i.e. acid-catalyzed substitution of *p*-xylene), 2,5-hexanedione (hydrolysis of DMF, see Figure S1), and furan-derived products and coke (condensation of 2,5 hexanedione, etc). This type of product distribution is similar to the one

[*] I. F. Teixeira,[+] B. T. W. Lo,[+] Dr. L. Ye, Prof. S. C. E. Tsang
Wolfson Catalysis Centre
Department of Chemistry
University of Oxford
Oxford OX1 3QR (UK)
E-mail: edman.tsang@chem.ox.ac.uk
P. Kostetskyy, Prof. G. Mpourmpakis
Department of Chemical Engineering
University of Pittsburgh
Pittsburgh, PA 15261 (USA)
E-mail: gmpourmp@pitt.edu
Dr. M. Stamatakis
Department of Chemical Engineering, University College London
Torrington Place, London WC1E 7JE (UK)
Prof. C. C. Tang
Diamond Light Source Ltd, Harwell Science and Innovation Campus
Didcot, Oxfordshire, OX11 0DE (UK)
[+] These authors contributed equally to this work.

Supporting information and ORCID(s) from the author(s) for this article are available on the WWW under: http://dx.doi.org/10.1002/anie.201604108.

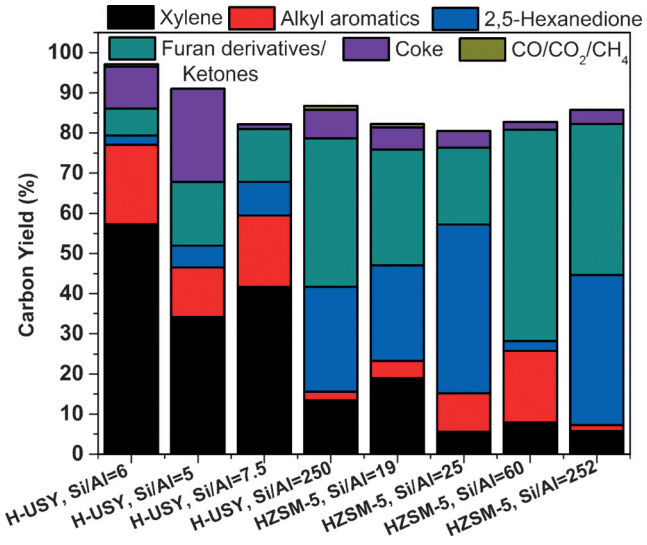

Figure 1. Carbon yield for DMF transformation into xylene (mainly *p*-xylene) and alkylaromatics catalyzed by different zeolites. Reaction conditions: temperature 300 °C, molar ratio ethanol/DMF 1:1 for 12 h in 100 mL reactor.

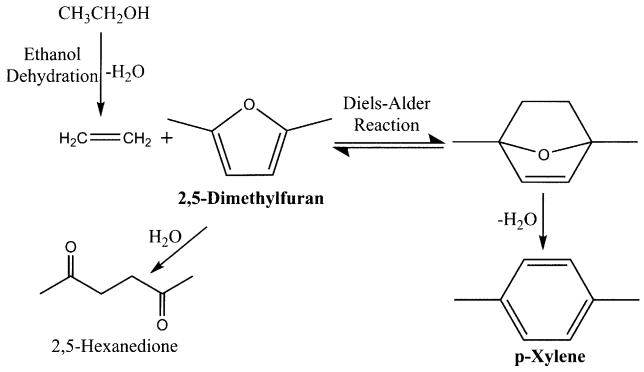

Scheme 1. A one-pot synthesis for *p*-xylene production from 2,5-dimethylfuran (DMF) and ethanol over zeolite.

originating from the DMF reacting with ethylene,[9–11] strongly suggesting that the in situ production of ethylene from ethanol is coupled with the Diels–Alder cycloaddition to DMF. Interestingly, the catalytic performance appears to be greatly influenced by the nature of zeolite and the acid content used (Figure 1). The zeolite HUSY-12 with intermediate acidic content (Si/Al = 6) gives the best carbon yield for aromatics compared with other Si/Al ratios. This HUSY also shows much higher yield than HZSM-5 of Si/Al = 19 or 25 with comparable Brønsted acid concentrations, suggesting HUSY has a more preferred pore structure (Figure 1 and Figure S2 and Table 1).

On the other hand, for ethylene used as a co-reactant, Williams et al. have demonstrated that their HY zeolite samples also give higher catalytic performance than the HZSM-5 samples, yielding about 50 % selectivity towards *p*-xylene (total aromatics of 60 %) in DMF/ethylene at 300 °C, without additional solvent inclusion.[9–11] Under comparable conditions, using ethylene as the co-reactant, our HUSY-12

Table 1: Properties of zeolites and rates of DMF conversions.

Catalyst	Si/Al ratio[a]	Brønsted acid sites[b] [mmol g^{-1}]	Total acid sites[b] [mmol g^{-1}]	Surface Area[c] [m^2 g^{-1}]	H-TOF[d] [10^2 h^{-1}]
H-USY	6	0.55	–	735	2.57
H-USY	5	1.1	–	650	0.23
H-USY	7.5	0.1	–	550	4.75
H-USY	250	0.1	–	620	5.02
H-ZSM-5	19	0.760	0.789	349	0.63
H-ZSM-5	25	0.310	0.344	311	1.50
H-ZSM-5	60	0.032	0.056	309	14.95
H-ZSM-5	252	–	0.002	329	–

[a] From ICP-MS. [b] From extinction coefficient.[14] [c] From BET over $0.05 < P/P_0 < 0.3$. [d] Rate of mol. DMF to mol. products per Brønsted acid site per hour.

sample (Si/Al = 6) with the same HY structure, but with partially destructed zeolite cavities and larger average pore sizes (ca. 2.1 nm), appears to give higher *p*-xylene (77 %) and total aromatic selectivity of 82 %, further enhancing the fraction of useful products (see Figure S3). When compared with ethanol as the source of dienophile, over the same HUSY-12 (Figure S3), the ethanol pathway exhibits even higher conversion. Despite the fact that a slightly lower selectivity to *p*-xylene (67 %) is obtained than that of using ethylene, the use of ethanol produces more alkylated aromatics (23 % against 5 % in ethylene reaction) over the HUSY-12 (Si/Al = 6), resulting to higher overall selectivity in the production of aromatics (90 %). Apart from the alkylated xylene products (for example, 1-ethyl-2,5-dimethylbenzene as ethyl substituted *p*-xylene) as in the case of ethylene, the use of ethanol also produces a very small quantity of aromatics with oxygen-containing substituent groups.

The conversion of DMF into aromatics over zeolites was also optimized for a range of parameters, such as time, temperature and ethanol/DMF ratio (Figures S4,S5). For example, the best ethanol/DMF ratio was in equimolar conditions (1:1) where almost complete conversions of DMF and ethanol were achieved to the *p*-xylene and derivative products based on their carbon balances (Figure S3). Using larger amounts of ethanol significantly promoted the formation of side products from DMF including the diketone and furan derivatives. The larger amount of 2,5-hexadione under excess ethanol might be explained by the increase in water concentration from the dehydration of ethanol, consequently shifting the reaction towards the formation of diketones and their condensed products. The study reflects the importance of a proper balance of ethanol dehydration versus Diels–Alder reactions over limited acid sites in the zeolite (see Figure S1), which reduces unnecessary consumption of ethanol for the tandem reactions. We were intrigued by the generally high rates of DMF conversion over the zeolites studied, using ethanol as the dienophile ($0.2–15 \times 10^2$ h^{-1}). Typically, the initial DMF conversion rate of

0.14 mol g cat^{-1} h^{-1} is achieved over HUSY-12 (estimated acid site concentration 4.4 mM) at 300 °C using ethanol, compared to 0.03 mol g cat^{-1} h^{-1} using ethylene (nearly 5 times more active) at the same conditions based on first two-hour evaluation (Table S2). More detailed kinetics studies were performed using liquid ethanol (0.14 mol) versus pressurized ethylene (40 bar, 0.45 mol) to react with 0.14 mol DMF over our HUSY-12 in a batch reactor under identical conditions. Despite the lower quantity of ethanol used, the reaction again showed a higher reaction rate (Figure 2, Figure S6). This is rather unexpected, since competition for limited acid sites in zeolite catalyst for dehydration of ethanol (to produce in situ ethylene), Diels–Alder cycloaddition and dehydration of oxa-norbornene to *p*-xylene (and substituted aromatics) should result in a lower rate relative to ethylene as a dienophile source. This observation may reveal important mechanistic details, which could lead to new ways of obtaining higher productivity of aromatics at greater selectivity from cyclo-addition of furans that is urgently needed in the practical catalytic biomass conversions.

The apparent activation energy for this reaction was also derived from an Arrhenius plot (Figure 2, insert). The value of 55.8 kJ mol^{-1} was significantly lower than the value using ethylene (ca. 100.0 kJ mol^{-1}),[11] giving $\Delta E_a \approx 44$ kJ mol^{-1} between the ethanol and ethylene routes. This implies that the reaction profiles involving the two dienophiles of different origins could be significantly different from each other.

Density functional theory (DFT), electronic structure methods were used to calculate the energy profile of the elementary steps of the two different reactions (*p*-xylene formation involving DMF + ethanol, or DMF + ethylene, demonstrated as black and red paths in Figure 3, respectively). In the ethylene route (red), the first step is the direct protonation of the DMF oxygen (from the zeolite proton; see also Table S1, see below for analysis on proton affinities). The subsequent steps that appear to determine the overall rate (showing higher barriers) are: i) the Diels–Alder (Diels–Alder^{+}, step II) cycloaddition and ii) the dehydration of the cyclo-adduct (oxa-norbornene via the C–O^{+} and C–H^{+} steps, IV and VI, respectively). This ethylene route has been originally analyzed by Caratzoulas et al.[9,15] with the same theoretical approach as our calculations. Due to their comparable energy barriers of the two steps, Dauenhauer and co-workers[9,10] have recently reported the Diels–Alder^{+} step being the rate-limiting if the Brønsted acid site concentration is above 2 mM, which can change to the dehydration step of cycloadduct at lower acid site concentration.

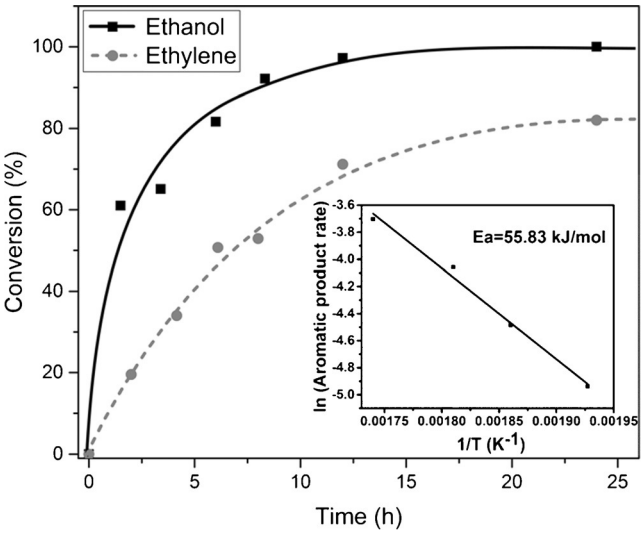

Figure 2. Kinetic data derived for 0.14 mole DMF transformation over 0.4 g zeolite HUSY-12 (Si/Al = 6) with ethylene generated in situ from ethanol (0.14 mole) versus pressurized ethylene (40 bar, 0.45 mole) in 100 mL at 300 °C. Inset: Arrhenius plot with calculated activation energy.

In our case of ethanol and DMF (black pathway of Figure 3), we observe a cascade of reactions: ethanol will be first preferentially protonated instead of DMF on the acid

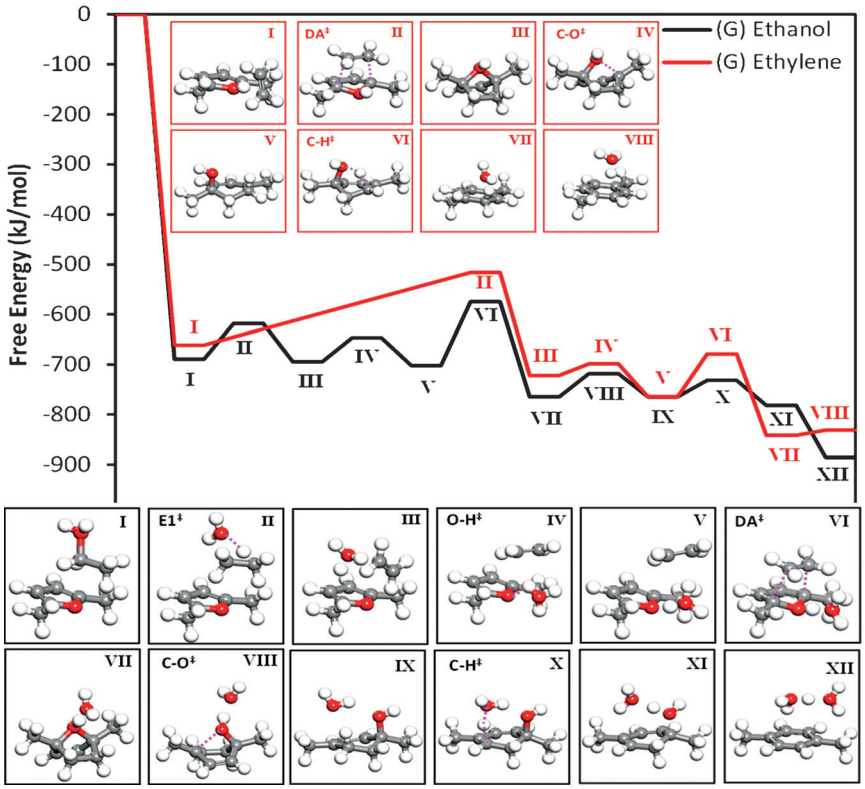

Figure 3. M06-2X calculated potential (free) energy landscape of two different pathways for *p*-xylene formation: ethanol route (black) and ethylene route (red), with relevant transition states shown as insets. The distinction of consequence between the two pathways lies on the preferred protonation of ethanol over DMF as a first step, compared to the protonation of DMF in the case of the ethylene route. All the energies are reported with respect to the energy of the reacting species and a proton at infinite separation. Pink dotted lines indicate hydrogen bonding.

site, followed by dehydration of the protonated ethanol (via E1 mechanism, step II) to ethylene and a protonated water molecule (hydronium ion, H_3O^+). The formation of this pronated water molecule plays a key role in the subsequent steps of the reaction mechanism. First, this hydronium forms a weaker hydrogen bond with the ring oxygen of DMF (O–H^+, step IV). At state V, the protonated water is stabilized through hydrogen bonds between the ethylene and the DMF with a configuration which is close to the Diels–Alder$^+$ transition state (step VI). This configuration is significantly different from that of state I in the ethylene (red) path since the LUMO of ethylene as dienophile comes closer to the HOMO of DMF as diene but with lower energy gap than that of ethylene route (Figure S7). Thus, these geometrical and electronic effects clearly result in decreasing the Diels–Alder barrier of the ethanol path by 11.2 kJ mol^{-1} as compared to the ethylene case (96.7 vs. 107.9 kJ mol^{-1}, see Table 2). In addition, the involvement of this water molecule further changes the entropic contributions at the Diels–Alder transition state in a way that favors the ethanol route (see Table 2 entropy (S) and free energy (G) values). Thus, lower free energy barriers are clearly obtained for ethanol (127.6 kJ mol^{-1}) compared to that of the ethylene route (145.2 kJ mol^{-1}) with the observed difference being well beyond the realms of DFT error at this level of theory (ca. 4 kJ mol^{-1}).[16] Also, this additional water produced from the dehydration of ethanol can facilitate the C–O cleavage (C–O^+), and particularly, the C–H dissociation (C–H^+) by mediating the hydrogen transfer with lower barriers (Figure 3, black line), forming the second water molecule, compared to the ethylene route (Figure 3, red line). The catalytic cycle is completed by a final proton transfer, to form *p*-xylene and a proton, stabilized by two water molecules. The corresponding free energies, enthalpies, and entropies of all the barriers involved in the two mechanisms are presented in Table 2. Furthermore, to assess the overall kinetic behavior of the two different mechanisms (ethanol vs. ethylene), we applied the energetic span model of Kozuch and Shaik[17] by using as input the free energy data presented in Table 2 and Figure 3. The calculated E-span barrier is 115.1 kJ mol^{-1} for the

Table 2: DFT-calculated barriers for the elementary steps in the ethanol and ethylene routes. Reported values include electronic energies, total free energies, enthalpies, and entropies at $T = 300\,°C$ (experimental temperature).

Pathway	Step	E_a [kJ mol^{-1}]	G_a [kJ mol^{-1}]	H_a [kJ mol^{-1}]	S_a [J mol K^{-1}]
Ethanol Route	E1$^+$	93.3	71.6	77.6	10.5
	O-H$^+$	36.4	47.3	38.5	−15.4
	Diels–Alder$^+$	96.7	127.6	96.3	−54.7
	C-O$^+$	59.9	46.9	53.6	11.6
	C-H$^+$	59.9	33.5	17.1	−28.5
Ethylene Route	Diels–Alder$^+$	107.9	145.2	109.0	−63.2
	C-O$^+$	33.7	23.4	25.4	3.5
	C-H$^+$	84.0	85.6	69.9	−27.4

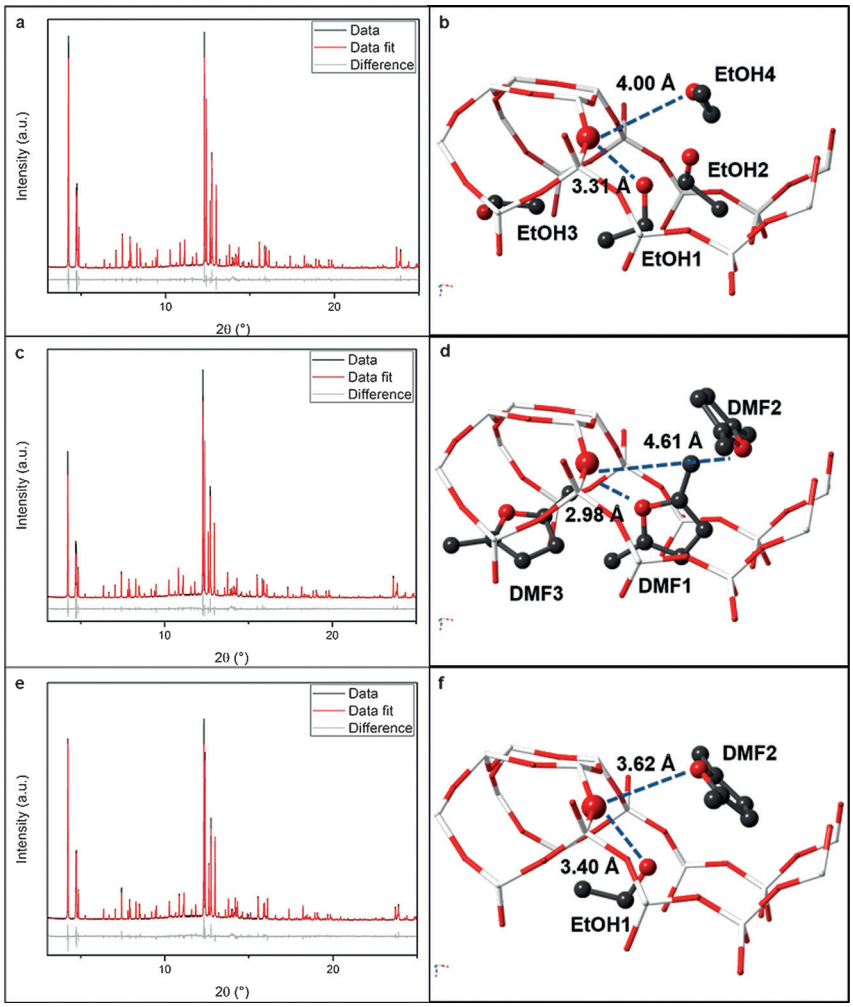

Figure 4. Rietveld refinement profiles of H-ZSM-5 pre-adsorbed with a) EtOH, c) DMF, and e) EtOH + DMF at 25 °C. Their derived atomic parameters of the SXRD data by Rietveld refinement method are summarized in Tables S3—S6, and the corresponding crystal models were constructed and displayed in b) EtOH, d) DMF, f) EtOH + DMF with the unit cell from [010] direction (straight-channel view). It shows clearly the 1st EtOH or DMF molecule on their own is first protonated by the cross-channel acid site (T6-OH) as $EtOH_2^+$ or $DMFH^+$ to give shorter distance (stronger interaction) at about O-(H^+)-O distance of 3.1 ± 0.2 Å before linking with weaker H-bonding of longer distance to their other EtOH or DMF molecules (in sinusoidal and straight channels of over O-(H^+)O distance of 4.0 Å, see Tables S3–S6), respectively, but the preferred protonation of EtOH in the cross-channel site is taking place first and forcing the DMF molecule to be linked by the weaker H-bonding when 1:1 EtOH and DMF are added. Atoms are represented in ball/sticks: white = Si/Al, red O (large dark red for acidic T6-OH), black C. No hydrogen atoms are plotted.

ethanol route and 155.4 kJ mol^{-1} for the ethylene. Although one would expect a deviation between the calculated E-span barriers and the experimentally obtained apparent activation energies (Figure 2), the calculated E-span activation energy difference between the two paths was found to be $\Delta E_a =$ 40.3 kJ mol^{-1}, which is in perfect agreement with the experimental observations ($\Delta E_a \approx 44$ kJ mol^{-1}).

One reason we observed this subtle rate-enhanced aromatics production from ethanol/DMF is because of the favored protonation of ethanol as the key step in decreasing the barriers of both the Diels–Alder and cycloadduct dehydration steps (Figure 3). It is crucially important to experimentally verify this preferred protonation in the pore of the zeolite. We have recently reported a new technique of using synchrotron X-ray powder diffraction (SXRD) combined with Rietveld refinement to elucidate adsorbate structures in zeolite. The alteration in scattering parameters of modified framework atoms by the molecule(s) enables the probing of adsorption geometries and interactions with the Brønsted acid site in terms of atomic distances and angles, within experimental error.[18] Thus, H-ZSM-5 sample containing one Al previously established at T6 position per asymmetric unit with the space group of *Pnma* was chosen (Table S3) to study its interactions with EtOH, DMF, and EtOH + DMF (1:1), respectively at their adsorbed states.

Notice that the uncertainty errors observed in atomic positions of these adsorbed molecules are, however, higher than that of rigid structural elements (O, Si) due to intrinsically higher degrees of freedom and higher isotropic temperature factor, Beq, (see Tables S4–S6). But, the generally low but acceptable Rwp and χ^2 values with closely fitted patterns suggest a good quality of refinement, indicating the reliability of the structural data within experimental errors. As seen in Methods section in the Supporting Information), greater than 4000 *hkl* reflections (more than 300 independent *hkl* reflections) in each case have been collected by SXRD, which allow a great number of structural variables (less than 170 in the refinements) to be refined in a satisfactory manner. From the derived refinement data, it is interesting to note that the two primary adsorbates (labelled as EtOH 1 and DMF 1) are found to locate in sinusoidal-straight cross-channel region of the H-ZSM-5 (Figure 4). As hydrogen atoms cannot be easily identified by SXRD, a simple way to gauge the interaction is by examining the atomic distances and angles between the lone pair electrons donated from the probe molecules and the framework oxygen atom carrying the acidic proton at the T6 position of the zeolite. It is clear that the strong acidic nature of the Brønsted acid between Al and Si in T6(Al)-O(H^+)-Si) indeed selectively protonates the adsorbate molecules to form primary protonated adduct cations (shorter O-(H^+)-O distance), followed by linking further adsorbate molecules via weaker H-bonding (longer O-(H^+)-O distance). It is exciting to confirm from Figure 4 that EtOH can be preferentially protonated over DMF by the acidic proton of the zeolite in 1:1 mixture of EtOH/DMF as evidenced by the proton affinity (PA) values of the reactants (see theoretical PA values[19] in Table S1, and ONIOM calculations in Figure S8 & Table S7). As a result, the DMF in the straight channel will be forced to interact with the $EtOH_2^+$ through a weak intermolecular H-bonding interaction, as depicted in Figure 3, state I. It should be noted that as shown in Table S1, the proton affinity follows the trend: ethanol > DMF > water > ethylene. This is consistent with the ideal proton flux that this reaction will be progressed with: first, ethanol has to protonate to dehydrate so it forms ethylene (dienophile supply) and protonated water, which further facilitates the Diels–Alder (lower HOMO–LUMO gap) and cycloadduct dehydration steps, as stated.

In summary, combining high-quality SXRD data and Rietveld refinement analysis with detailed kinetic measurements and high-level first principles calculations, we demonstrate that ethanol can act as a dienophile source for furan cycloaddition exhibiting substantial higher rates and lower reaction barriers than that of ethylene.[20] It is believed that the realization of higher production rates of aromatics in zeolites using bio-ethanol can underpin the rational design of zeolite catalysts and the employment of other co-substrates for this new improved process. The [4+2]-cycloaddition with different furans and dienophiles derived from biomass, including alkynes and alkenes in spatially defined zeolites may lead to tailored activity and stereochemistry.

Acknowledgement

We acknowledge the EPSRC (UK) and SINOPEC (China) for funding this project. We also thank University of Pittsburgh (US) for the computational support.

Keywords: biomass · cycloaddition · ethanol · structure elucidation · zeolites

How to cite: *Angew. Chem. Int. Ed.* **2016**, *55*, 13061–13066
Angew. Chem. **2016**, *128*, 13255–13260

[1] A. Brandt, J. Graesvik, J. P. Hallett, T. Welton, *Green Chem.* **2013**, *15*, 550–583.
[2] A. J. Ragauskas, C. K. Williams, B. H. Davison, G. Britovsek, J. Cairney, C. A. Eckert, W. J. Frederick, Jr., J. P. Hallett, D. J. Leak, C. L. Liotta, J. R. Mielenz, R. Murphy, R. Templer, T. Tschaplinski, *Science* **2006**, *311*, 484–489.
[3] R. Xing, A. V. Subrahmanyam, H. Olcay, W. Qi, G. P. van Walsum, H. Pendse, G. W. Huber, *Green Chem.* **2010**, *12*, 1933–1946.
[4] Y. Roman-Leshkov, J. N. Chheda, J. A. Dumesic, *Science* **2006**, *312*, 1933–1937; M. M. Wright, Y. Roman-Leshkov, W. H. Green, *Biofuels Bioprod. Biorefin.* **2012**, *6*, 503–520.
[5] D. M. Alonso, S. G. Wettstein, J. A. Dumesic, *Chem. Soc. Rev.* **2012**, *41*, 8075–8098.
[6] M. J. Climent, A. Corma, S. Iborra, *Green Chem.* **2014**, *16*, 516–547.
[7] J. S. Luterbacher, D. Martin Alonso, J. A. Dumesic, *Green Chem.* **2014**, *16*, 4816–4838.
[8] A. Zheng, Z. Zhao, S. Chang, Z. Huang, K. Zhao, H. Wu, X. Wang, F. He, H. Li, *Green Chem.* **2014**, *16*, 2580–2580.
[9] C. L. Williams, C.-C. Chang, P. Do, N. Nikbin, S. Caratzoulas, D. G. Vlachos, R. F. Lobo, W. Fan, P. J. Dauenhauer, *ACS Catal.* **2012**, *2*, 935–939.
[10] C. L. Williams, K. P. Vinter, C.-C. Chang, R. Xiong, S. K. Green, S. I. Sandler, D. G. Vlachos, W. Fan, P. J. Dauenhauer, *Catal. Sci. Technol.* **2016**, *6*, 178–187.

[11] C. L. Williams, University of Massachusetts Amherst (Amherst, MA 01003, United States), **2014**.
[12] Y.-T. Cheng, G. W. Huber, *Green Chem.* **2012**, *14*, 3114 – 3114.
[13] A. P. Kagyrmanova, V. A. Chumachenko, V. N. Korotkikh, V. N. Kashkin, A. S. Noskov, *XIX 4 International Conference on Chemical Reactors (CHEMREACTOR-19)* **2011**, *176 – 177*, 188 – 194; M. Zhang, Y. Yu, *Ind. Eng. Chem. Res.* **2013**, *52*, 9505 – 9514.
[14] C. A. Emeis, *J. Catal.* **1993**, *141*, 347 – 354.
[15] N. Nikbin, P. T. Do, S. Caratzoulas, R. F. Lobo, P. J. Dauenhauer, D. G. Vlachos, *J. Catal.* **2013**, *297*, 35 – 43.
[16] Y. Zhao, D. G. Truhlar, *Theor. Chem. Acc.* **2008**, *120*, 215 – 241.
[17] S. Kozuch, S. Shaik, *Acc. Chem. Res.* **2011**, *44*, 101 – 110.
[18] B. T. W. Lo, L. Ye, J. Qu, J. Sun, J. Zheng, D. Kong, C. A. Murray, C. C. Tang, S. C. E. Tsang, *Angew. Chem. Int. Ed.* **2016**, *55*, 5981 – 5984; *Angew. Chem.* **2016**, *128*, 6085 – 6088; L. Ye, B. T. W. Lo, J. Qu, I. Wilkinson, T. Hughes, C. A. Murray, C. C. Tang, S. C. E. Tsang, *Chem. Commun.* **2016**, *52*, 3422 – 3425.
[19] P. Kostestkyy, J. P. Maheswari, G. Mpourmpakis, *J. Phys. Chem. C* **2015**, *119*, 16139 – 16147.
[20] Reactions were carried out in a 100 mL, high-pressure, high temperature Parr reactor using zeolite catalysts provided by Sinopec. See Supporting Information for full details.

Received: April 27, 2016
Revised: June 6, 2016
Published online: August 4, 2016

